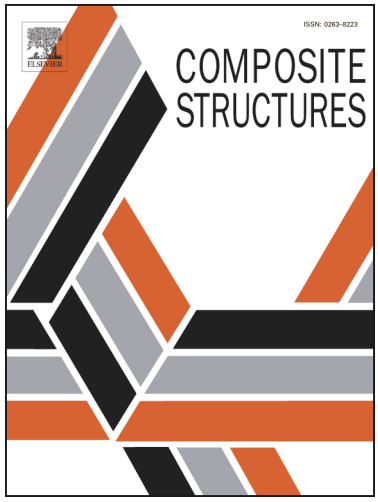

A novel understanding of the normalized fatigue delamination model for composite multidirectional laminates

Yu Gong, Wangchang Li, Hao Liu, Suzhen Yuan, Zhangming Wu, Chuanzeng Zhang

PII: S0263-8223(19)32294-9
DOI: https://doi.org/10.1016/j.compstruct.2019.111395
Reference: COST 111395

To appear in: *Composite Structures*

Received Date: 16 June 2019
Revised Date: 4 August 2019
Accepted Date: 9 September 2019

Please cite this article as: Gong, Y., Li, W., Liu, H., Yuan, S., Wu, Z., Zhang, C., A novel understanding of the normalized fatigue delamination model for composite multidirectional laminates, *Composite Structures* (2019), doi: https://doi.org/10.1016/j.compstruct.2019.111395

A novel understanding of the normalized fatigue delamination model for composite multidirectional laminates

Yu Gong[a,b,*], Wangchang Li[c], Hao Liu[a], Suzhen Yuan[d,*], Zhangming Wu[e,*], Chuanzeng Zhang[f]

[a] College of Aerospace Engineering, Chongqing University, Chongqing 400044, China

[b] Key Laboratory of Fundamental Science for National Defence of Aeronautical Digital Manufacturing Process, Shenyang Aerospace University, Shenyang 110136, China

[c] College of Materials Science and Engineering, Zhejiang University of Technology, Hangzhou, 310014, China

[d] College of opto electronic engineering, Chongqing University of Posts and Telecommunications, Chongqing 400065, China

[e] Cardiff School of Engineering, Cardiff University, Cardiff, CF24 3AA, UK

[f] Department of Civil Engineering, University of Siegen, Siegen, D-57068, Germany

Abstract: Normalized fatigue delamination models have been widely applied by researchers in the characterization of the fatigue delamination behavior of composite laminates. However, the inherent mechanism of this normalization method has not been explored. This study aims to present a physical understanding on the normalized fatigue delamination model from a viewpoint of energy. The fatigue delamination behavior is considered to be governed by the driving force and delamination resistance, and based on this principle the physical mechanism of the fatigue delamination is studied. A new physics-based normalized fatigue delamination model is proposed in this paper. In order to experimentally validate the proposed fatigue delamination model, mode I fatigue delamination tests are performed on double cantilever beam specimens to obtain the experimental data with different amounts of the fiber bridging. The results show that the normalized

* Corresponding author.
E-mail address: gongyu@cqu.edu.cn (Y. Gong), yuansuzhen@cqupt.edu.cn (S. Yuan), wuz12@cardiff.ac.uk (Z. Wu).

model is suitable to accurately characterize the fatigue delamination behavior of the composite laminates by using a single master curve. The master curve is finally employed as a standard approach to predict the fatigue results. Good agreement between the predicted and the experimental results is achieved, therefore it approves the applicability of the proposed fatigue delamination model in characterizing the fatigue delamination growth behavior.

Keywords: Composite laminates; Fatigue; Delamination growth; Fiber bridging

1 Introduction

Composite materials have been increasingly used in aerospace engineering from the secondary structures to the primary structures due to their higher strength to weight ratio compared with the traditional metallic materials. Due to the lack of the reinforcements along the thickness direction, delamination often occurs and therefore is a major form of damages in composite laminates [1]. When composite laminated structures are subjected to fatigue loading, delaminations may be initiated and developed due to manufacturing flaws and foreign object impacts, or interlaminar stresses may further evolve, resulting in stiffness degradation and finally catastrophic failure during its service life. In addition, other damage forms including matrix cracking and fiber pull-out/breakage may also be generated. These damage forms successively interact with each other under the fatigue loading. The diversity of the damage forms and the irregularity of the damage growth significantly increase the complexity and the difficulty of characterizing the fatigue delamination behavior accurately. Due to this complexity, composite structures are normally designed based on the assumption of no crack-growth and static strength criteria, which are considered to sufficiently cover the range of different fatigue damages. However, this concept can inevitably lead to conservative designs and significantly limit the full utilization of the potentials of composite materials in designing and applying advanced lightweight structures. Therefore, damage tolerance philosophy has been used in composite structural design, which has continuous demands

on a deep understanding of the damage mechanisms and reliable prediction models [2]. The model ability of accurately predicting the delamination growth behavior is important to avoid the improper design of composite structures, and is also useful to appropriately set the inspection intervals for damage monitoring in critical structural components [3].

The study of the fatigue delamination behavior in composite structures has attracted increasing concerns in the aviation industry in recent years. Researchers have proposed various methods based on the fracture mechanics concepts to characterize the fatigue delamination behavior. For example, the Paris model, $\mathrm{d}a/\mathrm{d}N=C[f(G)]^m$, and its different variants have been successfully employed to characterize the fatigue delamination behavior under specific scenarios [4]. In these models, the fatigue delamination growth rate $\mathrm{d}a/\mathrm{d}N$ is usually correlated to the strain energy release rate (SERR) or the stress intensity factors (SIFs), and the parameters in these Paris models are determined by fitting the experimental data. The maximum SERR $G_{\max}$ [5-7] or the SERR range ΔG [8,9] as the similitude parameter was usually employed to interpret the fatigue delamination behavior. However, the exponent m is large in this approach, which means that small uncertainties in the applied loading may result in large uncertainties (at least one order of magnitude) in the prediction of the delamination growth rate [10]. Therefore, the Paris laws with $G_{\max}$ or ΔG as the similitude parameter are difficult to be adequately applied for the design purposes of the composite materials and structures.

To lower the exponential term in Paris laws, the normalization method is proposed in this paper. Normalized similitude parameters including $G_{\max}/G_{\mathrm{c}}$ [11,12] and $G_{\max}/G_{\mathrm{c}}(a)$ [13,14] are used, where G_{c} and $G_{\mathrm{c}}(a)$ denote the constant fracture toughness and the R-curve of the fracture toughness, respectively. However, the intrinsic physical mechanism of this normalization method remains unclear. In addition, it is worth to point out that so far there is still no consensus on the detailed formulations of SERR and $f(G)$ in the Paris-type laws [15,16], which can result in controversy in the fatigue data interpretation, taking the stress ratio effects as examples [16,17].

Establishing an accurate fatigue delamination model is a great challenge confronted in the scientific and engineering community. Most of the previous studies applied quite general fatigue delamination models, which collocated all fatigue test data into a single curve. However, the intrinsic fundamental mechanism has never been well studied and explained so far. In this study, a physics-based fatigue delamination model is proposed based on a normalized similitude parameter which is expressed in terms of the driving force and the delamination resistance. The physical mechanisms of the driving force and resistance are demonstrated in Section 2. Mode I fatigue delamination tests are conducted by the double cantilever beam (DCB) test set-up, and the test results are presented in Section 3. The obtained experimental fatigue data are used to validate the proposed model in Section 4.

2 Normalized fatigue delamination model

Delamination growth in composite laminates depends strongly on the energy in the vicinity of a crack-tip. The energy can be categorized into two types: the driving energy and the resistance energy. The driving force for the growth of a crack (either static or fatigue loading) is related to the stress state near the crack-tip. Hence, the driving energy depends on the external factors such as the loading, stress ratio and mode mixity. On the other hand, the damage zone developed around the main crack-tip includes the plastic deformation or micro-cracking of the matrix which extends and leads to side cracks and fiber bridging [18-20]. The fiber bridging, delamination migration [21,22] and matrix failures will inevitably result in the energy dissipation. This behavior can be characterized by the fatigue delamination resistance, which is affected by the internal factors such as the interface, delamination length and material composition. Fig. 1 illustrates the basic principle for establishing the controlling parameter in a normalized fatigue delamination model from the energy point of view.

Regarding to the driving energy ΔG, currently, there exist two different expressions for the

definition [9,23,24], namely, G_{max}-G_{min} and $\left(\sqrt{G_{max}}-\sqrt{G_{min}}\right)^2$. Rans et al. [9] pointed out that the expression G_{max}-G_{min} is not based on any physical mechanism in the fracture process. They also demonstrated that this expression violates the superposition principle which is central to linear elastic fracture mechanics [9]. Based on the principle of similitude, they clarified that the driving energy should be defined as $\left(\sqrt{G_{max}}-\sqrt{G_{min}}\right)^2$ and this definition has been adopted by other researchers [25,26] . To illustrate the background of this definition, G is expressed as

$$G = \frac{P^2}{2b}\frac{dC}{da} \tag{1}$$

in terms of the specimen compliance. Here, P and b are the applied load and the specimen width, and a and C are the crack length and the specimen compliance, respectively. Considering an applied load P, which can be subdivided into two components P_1 and P_2, i.e. $P = P_1 + P_2$. By substituting this into Eq. (1) for a particular state (dC/da and b are constants), the following equations

$$\begin{aligned} G_1 = \frac{P_1^2}{2b}\frac{dC}{da},\ \ G_2 = \frac{P_2^2}{2b}\frac{dC}{da}, \\ G = \frac{\left(P_1+P_2\right)^2}{2b}\frac{dC}{da} = \left(\sqrt{G_1}+\sqrt{G_2}\right)^2 \end{aligned} \tag{2}$$

can be obtained. Therefore, for $\Delta P = P_{max} - P_{min}$, ΔG can be defined as

$$\Delta G = \frac{\left(P_{max}-P_{min}\right)^2}{2b}\frac{dC}{da} = \left(\sqrt{G_{max}}-\sqrt{G_{min}}\right)^2 \tag{3}$$

The distinction between the definitions of G_{max}-G_{min} and $\left(\sqrt{G_{max}}-\sqrt{G_{min}}\right)^2$ can be illustrated by the following equations

$$\begin{aligned} \left(\sqrt{G_{max}}-\sqrt{G_{min}}\right)^2 = \frac{1}{2b}\frac{dC}{da}\left(\Delta P\right)^2, \\ G_{max} - G_{min} = \frac{1}{2b}\frac{dC}{da}\left(\Delta P\right)\left(2P_{mean}\right) \end{aligned} \tag{4}$$

It can be seen that G_{max}-G_{min} is dependent on the amplitude load ΔP and the mean load P_{mean}.

However, $\left(\sqrt{G_{\max}}-\sqrt{G_{\min}}\right)^2$ is only dependent on the amplitude load, which is analogous to ΔK as a similitude parameter.

Regarding to the delamination resistance, most fatigue delamination models adopted the *R*-curve $G_c(a)$ to characterize the changing resistance against the delamination growth. However, the states of the fiber bridging under the fatigue loading may be different from that under the static loading, which has been confirmed experimentally by Stutz et al. [6] and Donough et al. [27]. This fact can be easily understood by the illustration in Fig. 2. Fatigue delamination will grow even when the SERR at the crack-tip is far lower than the corresponding fracture toughness. Therefore, for two different specimens (static and fatigue specimens) with the same crack growth length, the static specimen requires a larger displacement loading than that required by the fatigue specimen to fail [28], i.e. $d_s > d_f$. It results in a higher value of the crack-opening-displacement (COD) of the static specimen than that of the fatigue specimen, i.e. $\delta_s > \delta_f$. Different values of the COD indicate different bridging states. Hence, $G_c(a)$ cannot be regarded as the real changing resistance against the fatigue delamination growth. The concept of the fatigue delamination resistance $G_{cf}(a)$, which is the critical SERR for the crack propagation under fatigue loading [29], is adopted here to characterize the material resistance during a fatigue loading.

The effects of $G_{cf}(a)$ on the fatigue delamination growth curves are shown in Figs. 3 and 4. The dashed line in Fig. 3 presents the fatigue delamination resistance $G_{cf}(a)$. It depends on the delamination length, which is similar to the *R*-curve used in the static tests [30-32]. Suppose that two specimens are applied under different maximum displacement loadings d_1 and d_2, the ΔG values of the specimens will gradually decrease with the delamination growth. Since $d_1 \neq d_2$, the ΔG-a curves of these two specimens will not coincide. Therefore, the delamination length will be different ($a_1 \neq a_2$) for two specimens even if they have the same value of the ΔG, i.e. ΔG_e. Different delamination lengths lead to different values of the G_{cf}, i.e. $G_{cf}(a_1) \neq G_{cf}(a_2)$. Hence, the fatigue delamination growth rates of these two specimens will also be different even they have the same

value of the ΔG.

Fig. 4(a) shows a sketch plot of the da/dN-ΔG curve in double logarithmic coordinates for different loading displacements d_1 and d_2. Although the da/dN-ΔG curve at each value of $d_{\max}$ fits the traditional Paris law well, the traditional Paris law fails to characterize the delamination growth behavior for different values of $d_{\max}$. However, if the effect of G_{cf} is considered, the da/dN-$\Delta G/G_{\mathrm{cf}}$ curves will exhibit a linear behavior and reduce to a single line in double logarithmic coordinates for different values of $d_{\max}$, as shown in Fig. 4(b).

The above explanations present an understanding of the physical mechanism of the normalized fatigue delamination model from an energy point of view. Based on the previous discussions on the driving force and the delamination resistance, a physics-based normalized fatigue delamination model in terms of the fatigue delamination growth rate da/dN versus the normalized SERR range $\Delta g(a)$ is proposed which can be expressed as

$$\frac{da}{dN} = C\left(\Delta g(a)\right)^m = C\left(\frac{\left(\sqrt{G_{\max}(a)} - \sqrt{G_{\min}(a)}\right)^2}{G_{\mathrm{cf}}(a)}\right)^m \tag{5}$$

The $G_{\mathrm{cf}}(a)$ is the fatigue delamination resistance defined as the critical energy release rate during the fatigue crack growth at a certain delamination length a. Several methods have been proposed to calculate the G_{cf}, such as the static re-loading method and compliance method [28,29]. The parameters C and m in Eq. (5) are the fatigue constants. The SERR $G_{\max}(a)$ and $G_{\min}(a)$ of the DCB specimens under fatigue loading can be calculated using the modified beam theory [33], which are given by

$$G = \frac{3Pd}{2b\left(a + |\Delta|\right)} \tag{6}$$

where P and d are the applied load and the loading point displacement, respectively, b is the specimen width, and Δ is a correction factor for the crack-tip displacement and rotation [34], which can be experimentally determined by generating a least-square plot of the cube-root of the

compliance $C^{1/3}$ (C is the loading point displacement d divided by the applied load P), as a function of the delamination length a. The correction Δ is important for the evaluation of fracture toughness; thus the availability of its calculated value should be checked. For specimens with fiber bridging in this study, stresses in the bridging zone may cause obvious increase of flexure modulus and reduction of the measured C values. Thereby, $C^{1/3}$ values at the delamination length less than the notable bridging distance should be excluded from the linear fit.

3 DCB tests and results

3.1 Specimen descriptions

The DCB specimens are manufactured and tested to investigate the fatigue delamination behavior with the fiber bridging, and the experimental results are used to validate the normalized fatigue delamination model. The lay-up sequence of the specimens is $0_{16}//(+5/-5/0_6)_S$. The double slash '//' denotes the location of the Teflon film, which is used for the creation of the initial pre-crack during the fabrication process. The specimens are made from the T700 carbon/bismaleimide prepregs supplied by Beijing Institute of Aeronautical Material. The basic material elastic properties are as following: E_{11} = 130GPa, E_{22} = E_{33} = 10.4GPa, G_{12} = G_{13} = 6.36GPa, v_{12} = v_{13} = 0.3. An initial pre-crack is formed by inserting a thin Teflon film with a thickness of 25μm and a length of 35mm into the middle plane of the plates during the lay-up curing process. According to the supplier's manual, the cured plates are cut into specimens with a width of 25 mm, a length of 180 mm and a nominal thickness of 4.16 mm. All specimens are C-scanned to detect potential imperfections and only specimens without imperfections are used for the following delamination tests. C-scan detections are also performed for typical tested specimens in order to observe the uniformity of SERR width-wise distribution. And the C-scan images show that the difference of crack growth in the heart and both sides of the specimen is small. A quick-mounted hinge is adopted for applying the load to the specimens. Both edges of each specimen are coated with thin typewriter correction fluid to enhance the visibility of the delamination front during the fatigue tests.

3.2 Test procedures

All fatigue delamination tests are conducted on a MTS machine equipped with a 1.5kN load cell. In the fatigue tests, the displacement control mode is used at a frequency of 5Hz and a stress ratio of 0.1 as well as in room temperature and laboratory ambient conditions (23℃ and 50% RH). The load and displacement are recorded automatically using a data logger. The position of the crack-tip is observed by an instrumented microscope (JCXE-DK) with a precision of 0.01mm and the delamination length is measured at specific intervals. The experimental set-up is illustrated in Fig. 5.

Two specimens, F1 and F2, are fatigue tested two times with different applied displacements but with the same stress ratio. After the first test, the displacement is increased when the growth rate is lower than 10^{-7}mm/cycle, in order to avoid the crack retardation and long testing time. In this way, the fatigue delamination behavior with different amounts of the fiber bridging can be obtained. For each tests, the critical displacements corresponding to the delamination length can be firstly determined from the static results and the value of the applied displacement is chosen to be around 70% of the critical displacement. The fatigue data are analyzed using the normalized fatigue delamination model, Eq. (5). The model parameters C and m can be determined from a linear regression analysis of the fatigue data. A similar procedure is performed on other two specimens F3 and F4. The specimens F3 and F4 are also fatigue tested multiple times but at the same stress ratio. In each test, the fatigue delamination growth rate gradually decreases with the decrease of SERR until it almost retards. Then, the test is repeated with an increased applied displacements while keeping the same stress ratio. This procedure is repeated for multiple times until enough fatigue data are obtained. Multiple da/dN-ΔG curves can be obtained, with each curve corresponding to a specific fatigue pre-crack length, which is the delamination length at which that fatigue test is initiated. The test results from specimens F3 and F4 are applied for the model validation using the determined model parameters by results from specimens F1 and F2. A summary of the test matrix is

presented in Table 1.

The compliance method proposed in our previous studies [28,35,36] is adopted here to determine the fatigue delamination resistance curve. Detail discussions on the scheme of the compliance approach are presented and readers can refer to above literatures. The According to the compliance method, the value of the fatigue delamination resistance can be calculated by comparing with the compliance of the static and fatigue specimens at the same length of delamination. If the compliance of the static and fatigue specimens at a certain length of delamination, a_1, are the same. The value of the fatigue delamination resistance is numerically equivalent to the fracture toughness. Otherwise, the fatigue delamination can be calculated by Eq. (7).

$$G_{\mathrm{cf}}\left(a_1\right)=G_{\mathrm{c}}\left(a\left|_{m_{\mathrm{s}}(a)=m_{\mathrm{f}}\left(a_1\right)}\right.\right) \tag{7}$$

where the subscripts ‘‘f’’ and ‘‘s’’ indicate the fatigue and the static specimen, respectively. m_{f} and m_{s} are the slopes of the load-displacement curves for the fatigue and the static specimen, respectively.

In order to apply the compliance method, the fatigue tests are interrupted at around the point of the minimum displacement loading after a certain length of the delamination growth. Subsequently, a static displacement loading with a rate of 0.1mm/min is applied on the specimen until arriving 80% of the mean amplitude of the fatigue loading. The compliance of the fatigue specimen at the specific delamination length can be determined from the experimentally obtained load-displacement curve. Following that, the fatigue tests are continued.

3.3 Test results

Based on the aforementioned test procedure, a series of da/dN-ΔG curves have been obtained from the fatigue experiments, as shown in Fig. 6. For each curve, the da/dN data exhibit a good linear relationship with the ΔG in double logarithmic coordinates. The fatigue delamination behavior for F1-41.9mm is different from these for F1-36.8mm, F2-36.4mm and F2-40.3mm. This is because the amount of fiber bridging in the wake of crack tip is delamination length dependent. More bridging

fibers occur in F1-41.9mm and result in a lower fatigue delamination growth rate at the same values of ΔG. In addition, for different pre-crack lengths, the da/dN-ΔG curves are almost parallel to each other, which means that the pre-crack length hardly affects the slopes of the curves. All curves somewhat differ from each other due to the effect of the fiber bridging. This phenomenon illustrates that the da/dN curve is not the same at a given ΔG for the delamination growth with the effect of the fiber bridging, which is consistent with the discussion in Section 2. Thus, it is inappropriate to employ any single da/dN-ΔG curve, as shown in Fig. 6, to determine the fatigue delamination growth, which may cause overestimated or underestimated results. Furthermore, the exponent of the da/dN-ΔG from the case of specimen F1 with a pre-crack length of 41.9mm is obtained by the traditional Paris model for example. It is shown that the exponent value m is high as 17.75. If this value is applied for the fatigue delamination prediction, small uncertainties in the applied loading will result in large uncertainties. This also indicates that the ΔG is not an appropriate similitude parameter for characterizing the fatigue delamination growth with the effect of the fiber bridging.

The measured value of $G_{cf}(a)$ for the specimens studied is shown in Fig. 7. It can be seen that the $G_{cf}(a)$ increases with the growth of fatigue delamination. For comparison, the same fatigue data are interpreted with the normalized fatigue model, Eq. (5), as shown in Fig. 8. It can be found that all the data points are in good agreement with the results predicted by the proposed model. The fitted curve by Eq. (5) is also included in this figure as a single master curve, with the R-squared value being 0.74. Consequently, the $\Delta G/G_{cf}(a)$ can be considered as an appropriate similitude parameter for characterizing the fatigue delamination behavior. A linear regression analysis of the fatigue data reveals that the values of the coefficient C and the exponent m are 0.0182 and 7.29, respectively. The determined normalized model therefore can be written as

$$\frac{\mathrm{d}a}{\mathrm{d}N} = 0.0182\left(\frac{\Delta G}{G_{\mathrm{cf}}(a)}\right)^{7.29} \tag{8}$$

The value of the exponent m is much lower than that in the traditional Paris model. This feature is

important for the application of the normalized model in engineering designs. A smaller value of m indicates a weaker sensitivity of the da/dN curve to the similitude parameter, which is really beneficial for the accuracy improvement to predict the fatigue delamination behavior. Furthermore, once the master curve is established with a limited number of the tests, the fatigue delamination with different amounts of the fiber bridging can be well estimated. Therefore, the application of the normalized model can greatly reduce the testing workload and time in determining the fatigue delamination with fiber bridging, which has highly promising potentials in engineering applications.

4 Validation of the fatigue delamination model

From the discussions in Section 2 and Subsection 3.2, the normalized model is suitable to fairly characterize the fatigue delamination growth behavior of composite laminates. In order to provide extra evidence for its validation and accuracy, the model given by Eq. (8) is applied here to predict the fatigue delamination behavior in the specimens F3 and F4. The F3 and F4 specimens are repeatedly fatigue tested three or four times with the same stress ratio 0.1. The experimental da/dN-ΔG curves are shown in Fig. 9. To include the scatters in the fatigue test data, the 95% confidence interval of the experimental results is also calculated in accordance with the regression analysis. The predicted results by using Eq. (8) are also presented in Fig. 9 for the purpose of comparison. Pretty good agreements between the predicted and experimental results are observed in all the cases. The predicted results are located in or really close to the 95% confidence interval, and the predicted curve slopes are the same as the experimental ones, illustrating the effectiveness and robustness of the proposed normalized fatigue delamination model. Therefore, it can be concluded that the normalized model is suitable to predict the fatigue delamination growth accurately and effectively.

The variability in the mode I fatigue delamination growth curves is usually large and the normalization method can reduce the variability but did not eliminate it [37]. The specimens studied here are supplied by the Beijing Institute of Aeronautical Material and fabricated from the same

batch, in order to minimize the effect of specimen variation and inherent scatter. The delamination growth length and applied load can be precisely recorded by a microscope with a high precision of 0.01mm and a load cell with a small capacity, respectively. Our previous static and fatigue test results exhibit a relatively small variability and the high reliability [16,30]. Linear regression analysis for the obtained da/dN-ΔG curves in this study also shows a high coefficient of determination. To account for the possible variability, the 95% confidence intervals are provided in Fig. 9.

Additionally, it should be pointed out that the normalized fatigue delamination model is also valid for the delamination prediction without the effect of the fiber bridging. In this case, the $G_{cf}(a)$ is constant and equal to the initial fracture toughness, and the normalized model simplifies to the traditional Paris model. And it is know that the da/dN-ΔG curves for different applied displacements are supposed to lie on a single curve if no fiber bridging occurs in the delamination process. Thus, the normalized fatigue delamination model can be regarded as a generalized form of the Paris model for characterizing the fatigue delamination growth.

The proposed fatigue delamination model is only suitable for characterizing the linear growth rate domain of the fatigue delamination growth rate. By categorizing the influencing factors into two types, namely external and internal ones, the fundamental physical mechanism of the normalized fatigue delamination model is identified in terms of the driving force and the delamination resistance. This provides an ideal approach for establishing novel physics-based models to characterize the fatigue delamination behavior. The model proposed here is an initial attempt to develop accurate and efficient prediction methods for the fatigue delamination growth. It should be remarked here that the influencing factors on the fatigue delamination behavior are numerous, such as the stacking sequence, stress ratio, mode mixity, interface property, specimen geometry and loading type. Therefore, it is worthwhile to point out that the fatigue delamination resistance is not a material constant but specimen dependent. The study here is an initial step to

develop accurate and efficient prediction methods for the fatigue delamination growth. Further studies with more specimens tested and other material systems are necessary to be conducted in the future in order to have better understanding of these influencing factors on the fatigue delamination and provide necessary information for developing fatigue delamination growth model.

5 Crack paths and fracture surfaces

Some typical crack path photos of the tested specimens are presented in Fig. 10(a). From the view of the front side, it can be seen that the delamination predominantly grows along the mid-plane and the fiber bridging appears in the wake of the crack-tip. In addition, the failed fracture surfaces are examined via an optical microscope to further understand the delamination growth mechanism. Because all fracture surfaces are similar, only one typical fracture surface is illustrated here. Figs. 10(c)-(e) show the microscopic images taken from different locations on the failed delamination fracture surface. Fig. 10(c) demonstrates that the delamination initiates along the interface between the resin and the adjacent 5° fibers, although a small resin-rich region can be observed. The 0° or 5° fibers expose alternately along the width direction of the specimens. With the delamination growth, the exposed fibers are gradually "pulled out" and result in a high degree of the fiber bridging, as shown in Figs. 10(d)-(e). A widespread breaking of the bridging fibers can be observed on the fracture surface, which mainly result in an increasing delamination resistance due to the energy dissipated in the damage of the bridging fibers.

6 Conclusions

This study presents a physical understanding and interpretation on the normalized fatigue delamination model from the energy point of view. The normalized similitude parameters can be correlated to the driving force and delamination resistance, and the corresponding intrinsic mechanisms are discussed. A physics-based normalized fatigue delamination model is thus proposed to characterize the fatigue delamination behavior. The mode I fatigue delamination

behavior with the effect of the fiber bridging in the composite laminates is experimentally investigated. The crack paths and fracture surface photographs of the tested specimens illustrate the existence of significant fiber bridging during the delamination process, which provides helpful information for understanding the damage mechanism. The test results show that a master curve can be obtained if the $\Delta G/G_{cf}$ is adopted as the similitude parameter. The normalized fatigue delamination model can accurately characterize the fatigue delamination behavior of the composite laminates. The prediction performance of the normalized fatigue delamination model is also studied and approved. The good agreement between the predicted and experimental results clearly demonstrates the reliability and accuracy of the normalized fatigue delamination model proposed in this work. The normalized fatigue delamination model can be regarded as a more general form of the traditional Paris law, which is valid for the delamination growth with or without the fiber bridging.

Acknowledgements

This research work is supported by the National Natural Science Foundation of China, the Chongqing Natural Science Foundation (Project no. cstc2018jcyjAX0235), the Fundamental Research Funds for the Central Universities (Project no. 2019CDXYHK0001) and the Key Laboratory of Fundamental Science for National Defence of Aeronautical Digital Manufacturing Process of Shenyang Aerospace University (Project no. SHSYS2018001). Yu Gong also gratefully acknowledges the financial support from the German Academic Exchange Service (DAAD) to support his fellowship research at the Chair of Structural Mechanics, University of Siegen, Germany.

References

[1] L Zhao, Y Wang, J Zhang, Y Gong, N Hu, N Li. XFEM-based model for simulating zigzag delamination growth in laminated composites under mode I loading. Compos Struct 2017; 160: 1155-62.

[2] S Rubiera, A Argüelles, J Viña, C Rocandio. Study of the phenomenon of fatigue delamination in a carbon-epoxy composite under mixed mode I/II fracture employing an asymmetric specimen. Int J Fatigue 2018; 114: 74-80.
[3] LR LeBlanc, G LaPlante. Experimental investigation and finite element modeling of mixed-mode delamination in a moisture-exposed carbon/epoxy composite. Composites Part A: Applied Science and Manufacturing 2016; 81: 202-13.
[4] I Simon, L Banks-Sills, V Fourman. Mode I delamination propagation and R-ratio effects in woven composite DCB specimens for a multi-directional layup. Int J Fatigue 2017; 96: 237-51.
[5] M Hojo, K Nakashima, T Kusaka, M Tanaka, T Adachi, T Fukuoka, M Ishibashi. Mode I fatigue delamination of Zanchor-reinforced CF/epoxy laminates. Int J Fatigue 2010; 32: 37-45.
[6] S Stutz, J Cugnoni, J Botsis. Studies of mode I delamination in monotonic and fatigue loading using FBG wavelength multiplexing and numerical analysis. Compos Sci Technol 2011; 71: 443-9.
[7] M Shahverdi, AP Vassilopoulos, T Keller. Experimental investigation of R-ratio effects on fatigue crack growth of adhesively-bonded pultruded GFRP DCB joints under CA loading. Composites Part A: Applied Science and Manufacturing 2012; 43: 1689-97.
[8] W Hwang, KS Han. Interlaminar fracture behavior and fiber bridging of glass-epoxy composite under mode I static and cyclic loadings. J Compos Mater 1989; 23: 396-430.
[9] C Rans, R Alderliesten, R Benedictus. Misinterpreting the results: How similitude can improve our understanding of fatigue delamination growth. Compos Sci Technol 2011; 71: 230-8.
[10] Y Gong, L Zhao, J Zhang, N Hu. A novel model for determining the fatigue delamination resistance in composite laminates from a viewpoint of energy. Compos Sci Technol 2018; 167: 489-96.
[11] N Blanco, EK Gamstedt, LE Asp, J Costa. Mixed-mode delamination growth in carbon-fibre composite laminates under cyclic loading. Int J Solids Struct 2004; 41: 4219-35.
[12] I Jaeck, L Carreras, J Renart, A Turon, F Martin De La Escalera, Y Essa. Experimental methodology for obtaining fatigue crack growth rate curves in mixed-mode I-II by means of variable cyclic displacement tests. Int J Fatigue 2018; 110: 63-70.
[13] K Shivakumar, H Chen, F Abali, D Le, C Davis. A total fatigue life model for mode I delaminated composite laminates. Int J Fatigue 2006; 28: 33-42.
[14] H Chen, K Shivakumar, F Abali. A comparison of total fatigue life models for composite laminates. Fatigue Fract Eng M 2006; 29: 31-9.
[15] JA Pascoe, RC Alderliesten, R Benedictus. Methods for the prediction of fatigue delamination growth in composites and adhesive bonds-A critical review. Eng Fract Mech 2013; 112: 72-96.
[16] L Zhao, Y Gong, J Zhang, Y Wang, Z Lu, L Peng, N Hu. A novel interpretation of fatigue delamination growth behavior in CFRP multidirectional laminates. Compos Sci Technol 2016; 133: 79-88.
[17] S Stelzer, AJ Brunner, A Argüelles, N Murphy, GM Cano, G Pinter. Mode I delamination fatigue crack growth in unidirectional fiber reinforced composites: Results from ESIS TC4 round-robins. Eng Fract Mech 2014; 116: 92-107.
[18] Y Gong, L Zhao, J Zhang, Y Wang, N Hu. Delamination propagation criterion including the effect of fiber bridging for mixed-mode I/II delamination in CFRP multidirectional laminates. Compos Sci Technol 2017; 151: 302-9.
[19] Y Gong, L Zhao, J Zhang, N Hu. An improved power law criterion for the delamination propagation with the effect of large-scale fiber bridging in composite multidirectional laminates.

Compos Struct 2018; 184: 961-8.
[20] Y Gong, B Zhang, L Zhao, J Zhang, N Hu, C Zhang. R-curve behaviour of the mixed-mode I/II delamination in carbon/epoxy laminates with unidirectional and multidirectional interfaces. Compos Struct 2019; 223: 110949.
[21] Y Gong, B Zhang, SR Hallett. Delamination migration in multidirectional composite laminates under mode I quasi-static and fatigue loading. Compos Struct 2018; 189: 160-76.
[22] Y Gong, B Zhang, S Mukhopadhyay, SR Hallett. Experimental study on delamination migration in multidirectional laminates under mode II static and fatigue loading, with comparison to mode I. Compos Struct 2018; 201: 683-98.
[23] R Jones, S Pitt, AJ Bunner, D Hui. Application of the Hartman-Schijve equation to represent Mode I and Mode II fatigue delamination growth in composites. Compos Struct 2012; 94: 1343-51.
[24] RC Alderliesten, J Schijve, SVD Zwaag. Application of the energy release rate approach for delamination growth in Glare. Eng Fract Mech 2006; 73: 697-709.
[25] R Jones, AJ Kinloch, W Hu. Cyclic-fatigue crack growth in composite and adhesively-bonded structures: The FAA slow crack growth approach to certification and the problem of similitude. Int J Fatigue 2016; 88: 10-8.
[26] R Khan, R Alderliesten, S Badshah, R Benedictus. Effect of stress ratio or mean stress on fatigue delamination growth in composites: Critical review. Compos Struct 2015; 124: 214-27.
[27] MJ Donough, AJ Gunnion, AC Orifici, CH Wang. Scaling parameter for fatigue delamination growth in composites under varying load ratios. Compos Sci Technol 2015; 120: 39-48.
[28] J Zhang, L Peng, L Zhao, B Fei. Fatigue delamination growth rates and thresholds of composite laminates under mixed mode loading. Int J Fatigue 2012; 40: 7-15.
[29] L Peng, J Zhang, L Zhao, R Bao, H Yang, B Fei. Mode I delamination growth of multidirectional composite laminates under fatigue loading. J Compos Mater 2011; 45: 1077-90.
[30] L Zhao, Y Gong, J Zhang, Y Chen, B Fei. Simulation of delamination growth in multidirectional laminates under mode I and mixed mode I/II loadings using cohesive elements. Compos Struct 2014; 116: 509-22.
[31] L Zhao, Y Wang, J Zhang, Y Gong, Z Lu, N Hu, J Xu. An interface-dependent model of plateau fracture toughness in multidirectional CFRP laminates under mode I loading. Composites Part B: Engineering 2017; 131: 196-208.
[32] MM Shokrieh, M Heidari-Rarani, MR Ayatollahi. Delamination R-curve as a material property of unidirectional glass/epoxy composites. Mater Design 2012; 34: 211-8.
[33] S Hashemi, AJ Kinloch, JG Williams. Mechanics and mechanisms of delamination in a poly (ether sulphone)-fibre composite. Compos Sci Technol 1990; 37: 429-62.
[34] S Hashemi, AJ Kinloch, JG Williams. The effects of geometry, rate and temperature on the mode I, mode II and mixed-mode I/II interlaminar fracture of carbon-fibre/poly (ether-ether ketone) composites. J Compos Mater 1990; 24: 918-56.
[35] L Peng, J Xu, J Zhang, L Zhao. Mixed mode delamination growth of multidirectional composite laminates under fatigue loading. Eng Fract Mech 2012; 96: 676-86.
[36] Y Gong, L Zhao, J Zhang, N Hu, C Zhang. An insight into three approaches for determining fatigue delamination resistance in DCB tests on composite laminates. Compos Part B-Eng (2019), doi: https://doi.org/10.1016/j.compositesb.2019.107206.
[37] GB Murri.Evaluation of Delamination Onset and Growth Characterization Methods under Mode I Fatigue Loading. NASA/TM-2013-217966, 2013.

Figure Captions

Fig. 1. Scheme for the establishment of the normalized fatigue delamination model.

Fig. 2. Different applied displacements and CODs in the (a) fatigue and (b) static specimens with the same crack growth length.

Fig. 3. Illustration of the same ΔG value but different G_{cf} values.

Fig. 4. The relationship curves of (a) da/dN-ΔG and (b) da/dN-$\Delta G/G_{cf}$.

Fig. 5. Set-up for mode I fatigue delamination test.

Fig. 6. Plots of da/dN versus ΔG for the F1 and F2 specimens.

Fig. 7. The value of $G_{cf}(a)$ for the tested specimens.

Fig. 8. Plots of da/dN versus $\Delta G/G_{cf}$ for the F1 and F2 specimens.

Fig. 9. Predicted results and experimental data for the (a) F3 and (b) F4 specimens.

Fig. 10. Crack path and failed fracture surfaces.

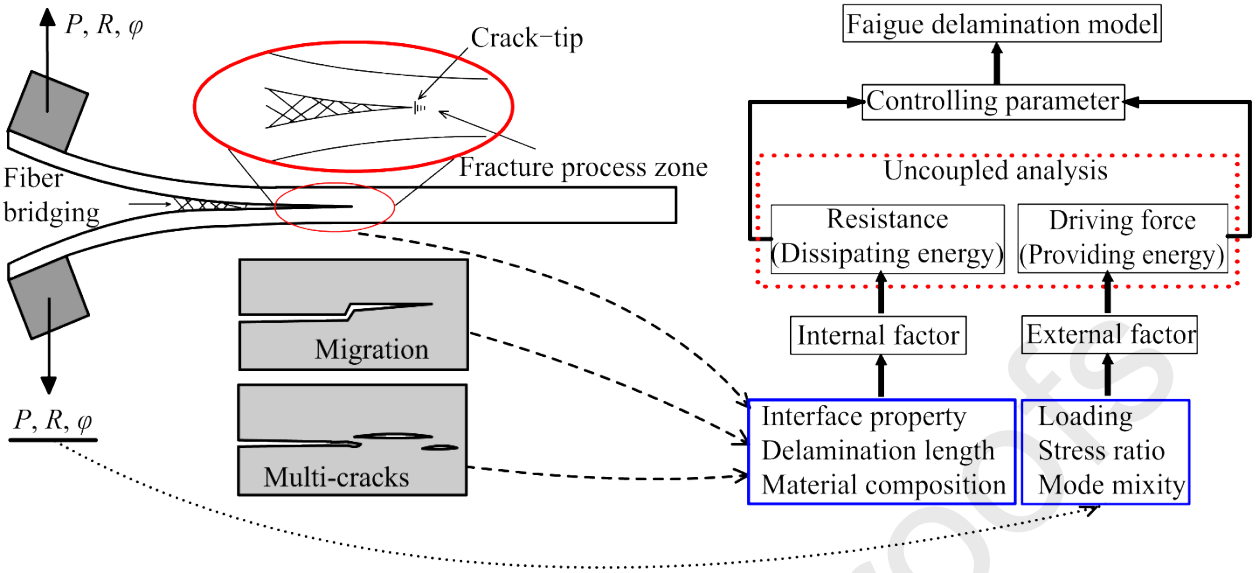

Fig. 1. Scheme for the establishment of the normalized fatigue delamination model.

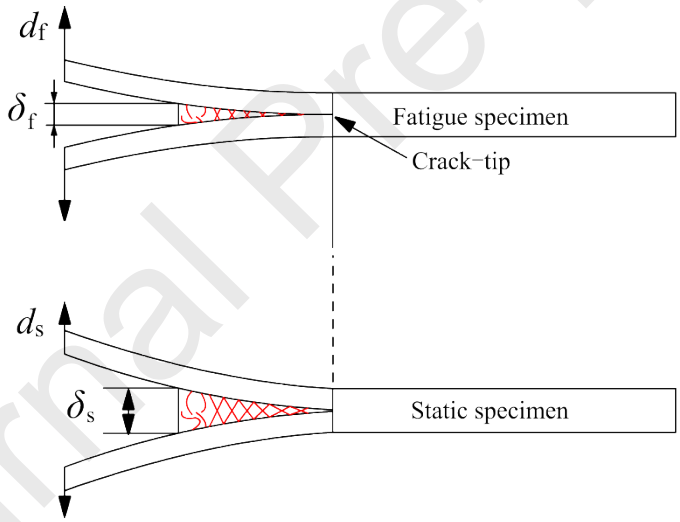

Fig. 2. Different applied displacements and CODs in the (a) fatigue and (b) static specimens with the same crack growth length.

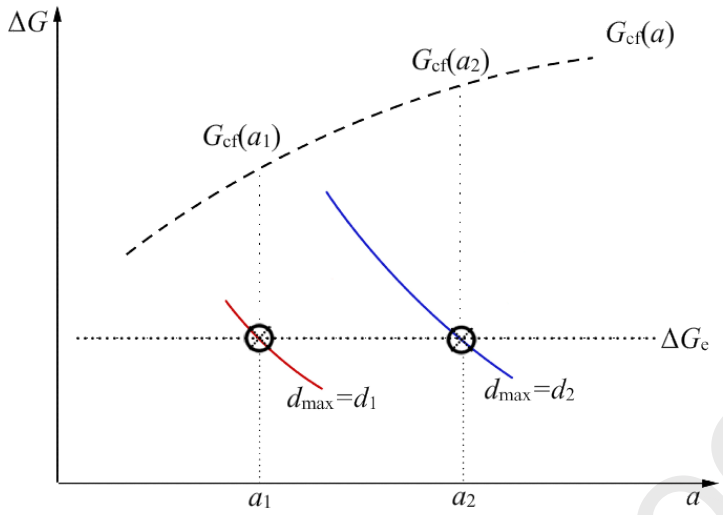

Fig. 3. Illustration of the same ΔG value but different G_{cf} values.

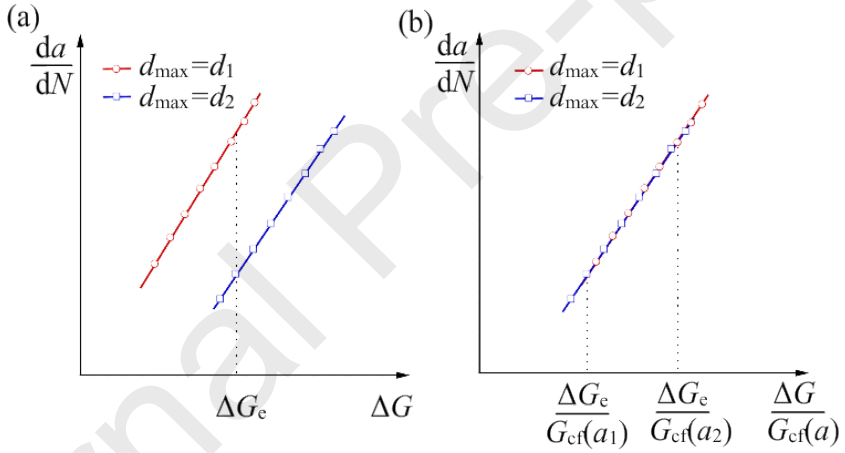

Fig. 4. The relationship curves of (a) da/dN-ΔG and (b) da/dN-$\Delta G/G_{cf}$.

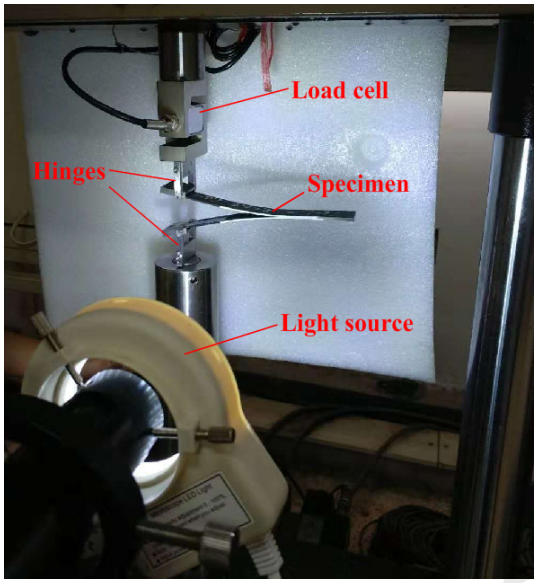

Fig. 5. Set-up for mode I fatigue delamination test.

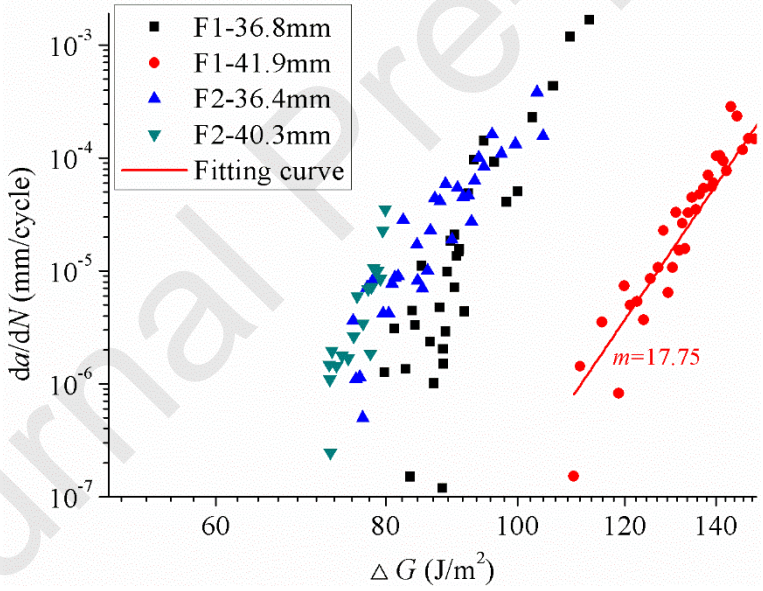

Fig. 6. Plots of da/dN versus ΔG for the F1 and F2 specimens.

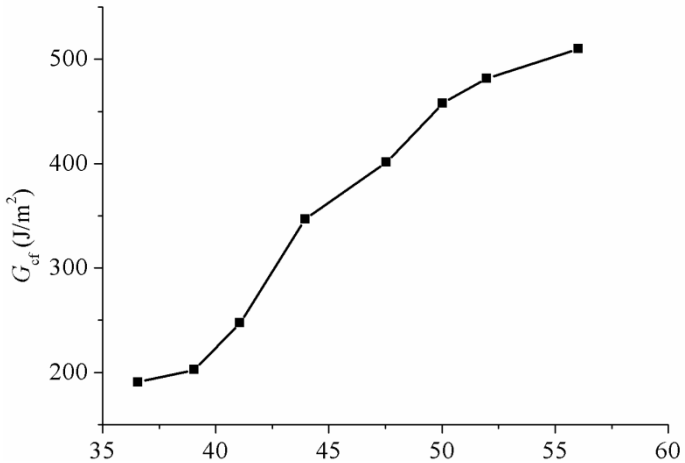

Fig. 7. The value of $G_{cf}(a)$ for the tested specimens.

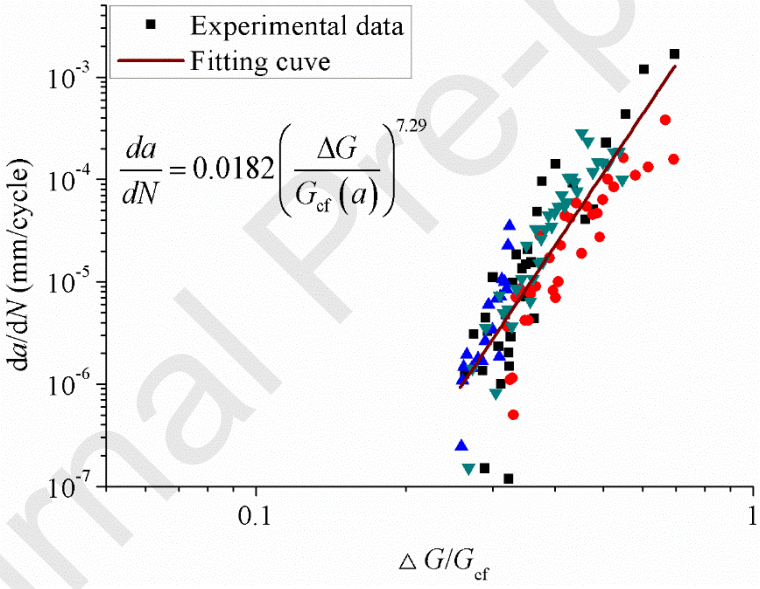

Fig. 8. Plots of da/dN versus $\Delta G/G_{cf}$ for the F1 and F2 specimens.

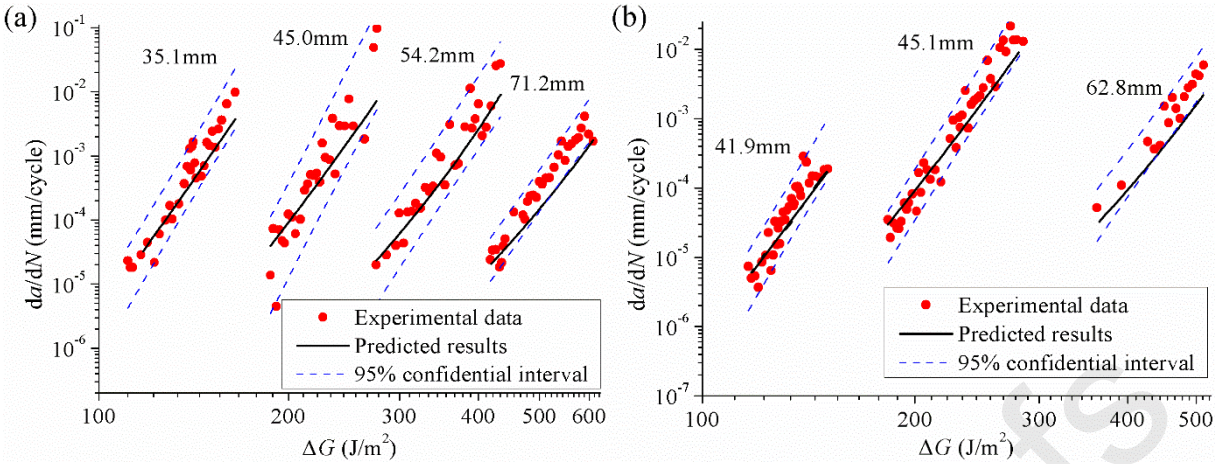

Fig. 9. Predicted results and experimental data for the (a) F3 and (b) F4 specimens.

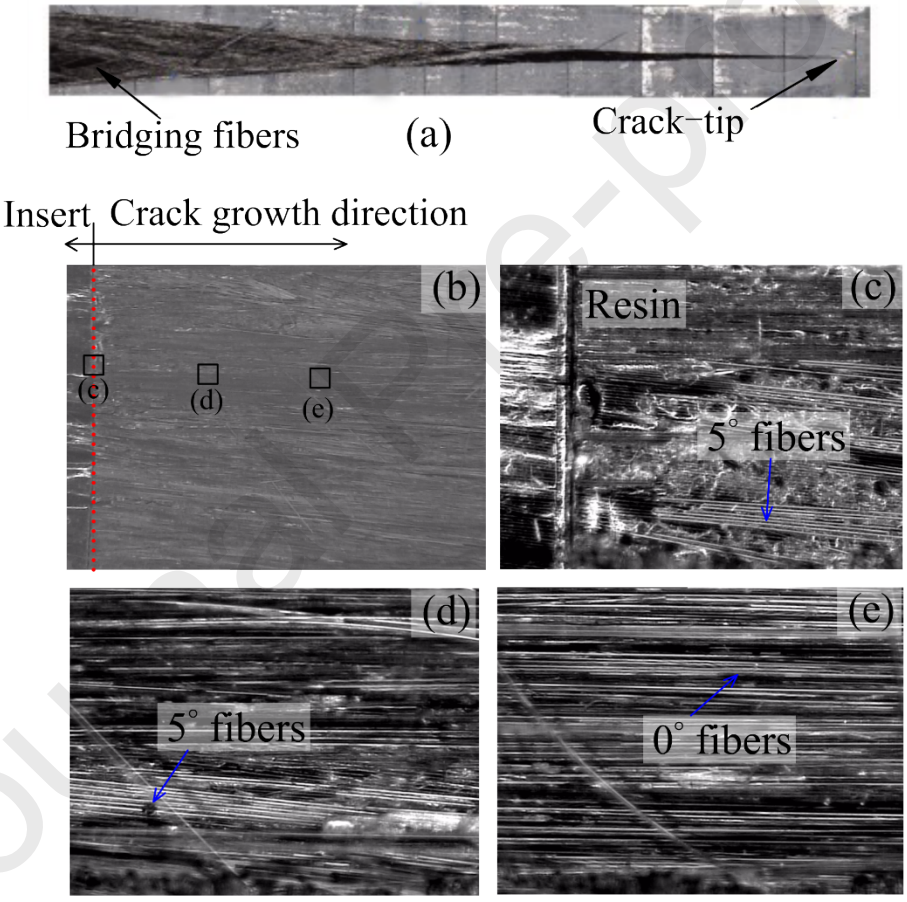

Fig. 10. Crack path and failed fracture surfaces.

Table Captions

Table 1 Fatigue test matrix.

Table 1 Fatigue test matrix.

Specimen no.	Stress ratio	Pre-crack length (mm)
F1	0.1	36.8mm, 41.9mm
F2		36.4mm, 40.3mm
F3		35.1mm, 45.0mm, 54.2mm, 71.2mm
F4		41.9mm, 45.1mm, 62.8mm